Hindawi
Geofluids
Volume 2022, Article ID 3835647, 11 pages
https://doi.org/10.1155/2022/3835647

Research Article

Impact of Dynamic Elastic Modulus on Coal Permeability: Modeling and Analysis

Jia Kong[1,2], **Baiquan Lin**[1,2], **Chuanjie Zhu**[1,2], **Ting Liu**[1,2] and **Xiangguo Kong**[3]

[1]*Key Laboratory of Coal Methane and Fire Control, Ministry of Education, China University of Mining and Technology, 221116, China*
[2]*School of Safety Engineering, China University of Mining & Technology, Xuzhou 221116, China*
[3]*Xi'an University of Science and Technology, Xi'an 710054, China*

Correspondence should be addressed to Baiquan Lin; lbq21405@126.com

Received 4 March 2022; Accepted 1 April 2022; Published 13 April 2022

Academic Editor: Wen-long Shen

Coalbed methane is a kind of high-quality clean energy. The underground gas drainage can achieve the efficient utilization of coalbed methane. Permeability is the key factor affecting gas drainage. At present, permeability research mainly considers the effect of gas adsorption-induced matrix swelling deformation as well as the effective stress. However, experiments indicate that the variation of pore pressure has an impact on the mechanical properties of coal, which further changes the coal permeability. Due to the differences between the theory and experimental results, firstly, the dynamic elastic modulus model was established in this paper. Then, an experiment was conducted to prove that the elastic modulus of coal-containing gas decreases with the increasing gas pressure. On this basis, a permeability model considering internal swelling deformation was constructed. Finally, the rationality of the model was validated through the laboratory experiment. Finally, through analyzing the influence of key parameters on the evolution law of permeability, we find that the parameters have three different impacts on permeability. The new permeability model is more accurate in predicting coalbed methane production capacity. The result can provide a theoretical basis for the research of the multifield coupling process during gas drainage.

1. Introduction

Coalbed methane (CBM) is a kind of hydrocarbon gas existing in coal measure strata [1, 2]. It is not only the high-quality clean energy with high thermal efficiency but also a greenhouse gas, causing gas outbursts, gas exploration, and other accidents [3–6]. The CBM reserves in the world are estimated at 84-262 trillion cubic meters, about 50% of the conventional natural gas resources [7]. Gas control is the most commonly used method for commercial production of CBM, which is of great significance for economic development, environmental protection, mining safety, and efficient utilization of coalbed methane resources [8–10].

Nowadays, gas control mainly adopts gas extraction, mine ventilation, etc. [11–17]. The permeability of coal reservoirs is the key factor that affects the adsorption/desorption, diffusion, and seepage of CBM. Therefore, mastering the evolution law of coal permeability is significant to methane extraction and the prevention of coal and gas outbursts. The previous studies focused on the influences of the competitive effect of gas adsorption-induced/desorption-induced matrix deformation and effective stress on permeability. Based on the theoretical study of uniaxial strain, Gray firstly established a coal permeability model which considered the matrix shrinkage [18]. Palmer and Mansoori developed the P&M model that incorporated the effects of matrix shrinkage and effective stress [19]. In addition, the P&M model matched well with the field test result of San Juan Basin and was widely used. Assuming that the volumetric strain caused by gas desorption changed the coal seam horizontal stress, which eventually altered the coal seam permeability, Shi and Durucan built the S&D model [20]. Based on the matchstick model, Liu and Rutqvist proposed the concept of a "matrix bridge" [21]. Under the condition of uniaxial strain and constant confining pressure, they introduced the internal swelling coefficient to quantify the interactive

relationship between the matrix and fractures, and a new theoretical model was established.

It is believed that coal permeability is affected by coal matrix swelling/shrinkage and effective stress [22–27]. The mechanical properties of coal have a significant impact on effective stress; therefore, coal permeability is also affected by the mechanical properties of coal. In the previous studies, the mechanical parameters of coal and rock samples were assumed to be constant. However, it has been suggested that the mechanical parameters of coal are variable, which is related to gas adsorption based on previous studies. Mishra and Dlamini studied the coal elastic modulus and deformation law when injecting gas into the coal [28]. They believed that the change of confining pressure caused by adsorption deformation is the main reason which gives rise to the variation of elastic modulus. Masoudian et al. found that CO_2 reduces the coal elastic modulus and strength. Moreover, this influence is reversible [29]. After adsorbing gas, the change of dual pore structure enhances the plastic deformation capacity of the coal. Wang et al. found that methane changes the coal elastic modulus and strength mainly by affecting the effective confining pressure and quick release of gas expansion energy [30].

Based on the previous studies, it is known that the mechanical properties of coal during methane extraction are dynamic. Although numerous models have been developed to characterize the permeability evolution, the impact of dynamic mechanical properties on coal permeability has not been completely understood and fully considered in the permeability models. The elastic modulus is a critical mechanical parameter of coal. In comparison with the previous studies, this paper proposes the third path to study the evolution law of coal permeability by introducing the concept of dynamic elasticity modulus, as shown in Figure 1.

In this study, the triaxial seepage test system was established to conduct the triaxial compression tests and the coal permeability experiments under different methane pressure. Moreover, we analyzed the influence of methane pressure on elastic modulus and built a mathematical model of dynamic elastic modulus based on the experimental results. A dynamic coal permeability model was then established, and the model was validated through laboratory tests. The results suggest that the new permeability model is more accurate in predicting CBM production capacity and helps the reasonable gas extraction borehole arrangement in the coal mine. The results can also provide a theoretical basis for the research of the multifield coupling process during methane extraction.

2. Experimental Methodology

2.1. Sample Preparation. The two types of coal, including bitumite (GSXB) collected from the Xinbei coal mine located in the northwest of China and anthracite (GZLH) collected from the Linhua coal mine located in the southwest of China, are taken as the experimental coal samples for experimental studies of dynamic elastic modulus and dynamic permeability model. The maceral and vitrinite reflectance analyses of specimens are listed in Table 1. For triaxial seepage tests, the samples with the size of $\Phi 50 \times 100$ mm were cored from large block coal, perpendicular to the bedding.

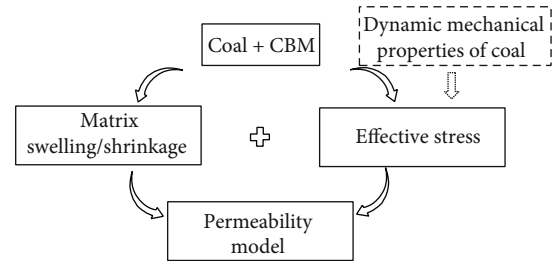

Figure 1: Conceptual graph of gas-solid coupling paths of coal and gas.

2.2. Sample Characterization. As mentioned earlier in this paper, the mechanics of methane-saturated coal is closely related to its gas adsorption capacity, and the gas adsorption capacity of coal is affected by its pore structure characteristics [31–33]. To assess the pore structure characteristics of coal samples, a nitrogen adsorption/desorption experiment and a nuclear magnetic resonance (NMR) experiment were conducted.

2.2.1. Nitrogen Adsorption/Desorption. To assess the pore structure characteristics of two samples, liquid nitrogen adsorption/desorption experiments were conducted. The liquid nitrogen adsorption and desorption curves are presented in Figure 2. The pore structure characteristics of samples were measured using powdered coal particles that passed through an 18~25 millimeter. Figure 2 illustrates that the nitrogen adsorption of coal increases slowly under low relative pressure. As the pressure increases, the isotherms between the adsorption and desorption had a hysteresis effect. The appearance of the adsorption hysteresis loop mainly depends on the capillary condensation that occurs on the solid surface [34, 35]. Finally, the nitrogen adsorption of coal increases fast under high relative pressure. The pore structure characteristics of the two samples are shown in Table 2. The pore volume of GSXB is 0.009 mL/g and the specific surface area is 6.0835 m^2/g which is relatively larger than 0.0055 mL/g and 2.3661 m^2/g of GZLH, respectively, which can provide broad spaces for gas adsorption.

2.2.2. NMR Measurements. To analyze the coal pore distribution, nuclear magnetic resonance (NMR) experiments were conducted. In the magnetic field, the hydrogen atoms present within the fluid can be detected by the transversal relaxation time (T_2); thus, the pore properties can be analyzed [36]. T_2 can be expressed as [37]

$$\frac{1}{T_2} = \rho \times \frac{S}{V} = \frac{a}{r}, \tag{1}$$

where ρ is a constant representing the transverse relaxation strength, S is the pore surface, V is the pore volume, r is the pore radius, and a is a pore shape factor.

It can be seen from Equation (1) that larger pores have longer T_2, and the higher the T_2 spectrum, the more the

Table 1: Raw coal properties.

Type	Coal rank	Vitrinite reflectance $R_{o,max}$ (%)	Proximate analysis (wt, %)				Coal maceral composition (%)			
			M_{ad}	A_d	V_{daf}	FC_{ad}	V	I	L	M
GSXB	Bituminous	1.45	2.51	9.70	38.54	55.49	65.89	31.51	—	2.6
GZLH	Anthracite	2.86	2.14	11.04	5.81	83.79	60.33	35.37	—	4.3

Notes: M_{ad}: moisture, air-drying basis; A_d: ash yield, air-drying basis; V_{daf}: volatile matter dry ash-free basis; FC_{ad}: fixed carbon content, air-drying basis; V: vitrinite; I: inertinite; L: liptinite; M: mineral.

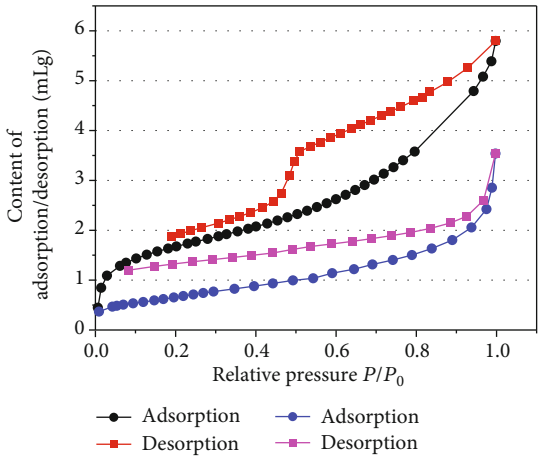

Figure 2: Nitrogen adsorption/desorption curves.

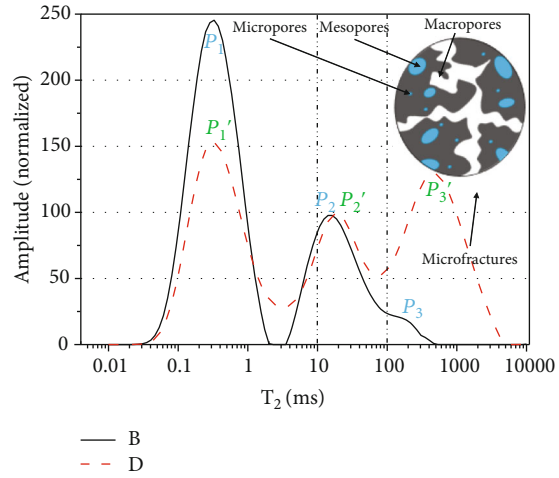

Figure 3: Results of nuclear magnetic resonance (NMR) experiments.

Table 2: Results of low-temperature nitrogen adsorption experiments.

Coal samples	GSXB	GZLH
Pore volume (mL/g)	0.009	0.0055
Specific surface area (m^2/g)	6.0835	2.3661
Mean pore size (nm)	5.9176	9.2980

pores. In addition, continuity between T_2 spectrum peaks represents the pore connectivity [38]. For coals, $T_2 < 10$ ms corresponds to micropores and 100 ms corresponds to macropores [39].

Figure 3 illustrates the coal pore distributions of GSXB and GZLH. The T_2 spectrum of GSXB consists of three separated peaks (i.e., P1, P2, and P3), indicating a large number of micropores and a small number of mesopores and macropores. Compared with the T_2 spectrum of GSXB, GZLH has the same trend. In contrast, of GZLH is lower, P_2' of GZLH is roughly equivalent to GSXB, and P_2' is higher, which indicates that the GZLH has more macropore and mesopore. The free fluids mainly migrate in macropores, which may result in the higher permeability of GZLH. The continuity between T_2 spectrum peaks of GZLH is better, which is a strong indication that micropores, mesopores, and all macropores are interconnected. In conclusion, GZLH has more macropores and fewer micropores, and this kind of unique feature makes GZLH have higher permeability and a lower adsorbability.

2.3. Experimental Procedure. The experiment system was established, which consists of a loading system, strain monitoring system, and flow acquisition system, as is shown in Figure 4.

Prior to each test, the samples were dried at 100°C for 24 h in a drying oven, and then, they were put into the core holder. The sample was degassed in the core holder under vacuum conditions at 30°C for 24 h. In the process of the test, a constant confining pressure of 5.0 MPa was used for the triaxial tests. The water pressure inside the triaxial cell was provided from a pressure controller. The methane was supplied from a high-pressure CH_4 cylinder with a maximum pressure of 13.0 MPa. According to the previous studies, the mechanical strength and elastic modulus of coal gradually decrease with the pore pressure increase in a certain range [29]. For example, the elastic modulus of coal does not change with increasing the CO_2 pressure from 8.0 MPa to 16.0 MPa [40]. For the same reason, the elastic modulus of coal also changes in a certain methane pressure range. Besides, the adsorption capacity of coal with respect to carbon dioxide is greater than that of methane. Therefore, the experimental methane pressures were set as 0, 1, 2, 3, and 4 MPa. Finally, the elastic modulus tests and the permeability of methane-saturated coal tests were conducted.

3. Modeling

3.1. Elastic Modulus Model. It is believed that gas adsorption on coal will result in the decrease of elastic modulus and

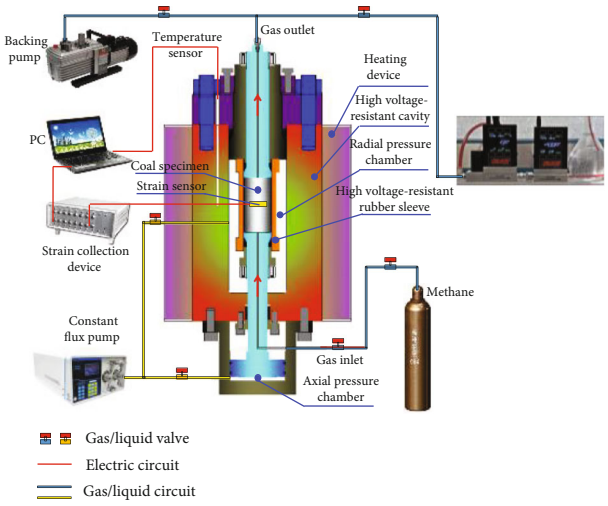

Figure 4: Schematic illustration of the saturation and triaxial setup.

strength of coal [41–43]. Therefore, it can be assumed that the variation of elastic modulus with pore pressure can be represented by the Langmuir model [29]. The elastic modulus defined in this work is different from that in the previous studies.

$$E_{CH_4} = E - \Delta E, \tag{2}$$

where E is the elastic modulus of gas-free coal (E) and E_{CH_4} is the elastic modulus of methane-saturated coal (E_{CH_4}). The decrease of elastic modulus caused by gas adsorption can be given as [29]

$$\Delta E = \frac{\Delta E_{max} \times P}{P_E + P}, \tag{3}$$

where P is the gas pressure, ΔE_{max} is the maximum decrease in the elastic modulus (associated with the maximum adsorption), and P_E is a curve-fitting parameter that is similar to the Langmuir pressure defined in Langmuir isotherm.

3.2. Permeability Model. To quantitatively analyze the influence of dynamic elastic modulus on permeability, the pore structure of coal was simplified. The typical simplified models mainly included the cube model, the sphere model, the capillary model, and the matchstick model [18, 44–46]. In this paper, the cube model containing a "coal matrix bridge" was proposed, which is composed of matrix blocks of size L_m and fractures with an aperture L_f. The matrix blocks are connected by the "coal matrix bridge" [47].

3.2.1. Gas Adsorption-Induced Swelling Deformation. Due to the "coal matrix bridge", the matrix deformation is impeded, which also reduces the fracture deformation. Therefore, only a part of gas adsorption-induced coal matrix deformation changes the fracture aperture, while the rest alters the volume of coal mass. In Figure 5(c), the light grey area represents the volume before adsorbing. The dark grey area surrounded by the dotted line is the deforming volume after adsorbing. It can be seen that matrix deformation (ΔL_m^S) consists of fracture deformation (ΔL_f^S) and coal mass deformation (ΔL_b^S). To quantify the adsorption-induced fracture deformation, the internal swelling coefficient f $(0 < f < 1)$ is introduced to represent the ratio of adsorption-induced fracture deformation to matrix deformation. Based on the simplified model,

$$\begin{aligned} \Delta L_f^S &= f\Delta L_m^S, \\ \Delta L_b^S &= (1-f)\Delta L_m^S. \end{aligned} \tag{4}$$

In this paper, we assume that the changing size of the matrix contains fracture deformation and coal mass deformation. For $L_f << L_m$, the strain increments of fracture volume and bulk volume caused by gas adsorption can be written as

$$\Delta\varepsilon_f^S = -\frac{3\Delta L_f^S}{L_f} = -\frac{3f\Delta L_m^S}{L_f} = -\frac{L_m}{L_f} f\Delta\varepsilon_m^S, \tag{5}$$

$$\Delta\varepsilon_b^S = -\frac{3\Delta L_b^S}{L_b} = -\frac{3(1-f)\Delta L_m^S}{L_m + L_f} = (1-f)\Delta\varepsilon_m^S. \tag{6}$$

Under the unconstrained state, the matrix swelling strain caused by gas adsorption $\Delta\varepsilon_m^S$ satisfies the Langmuir-type equation [19, 20].

$$\Delta\varepsilon_m^S = \varepsilon_L\left(\frac{p_m}{p_L + p_m} - \frac{p_{m0}}{p_L + p_{m0}}\right). \tag{7}$$

3.2.2. Deformation Caused by Effective Stress. The effective stress law of dual-porosity medium can be expressed as [48]

$$\sigma_e = \sigma - \left(\alpha p_f + \beta p_m\right)\delta_{ij}, \tag{8}$$

where σ_e is effective stress (MPa); σ is the total stress (MPa); δ_{ij} is Kronecker delta tensor; p_f is fracture gas pressure (MPa); p_m is matrix gas pressure (MPa); α and β are Biot effective stress coefficients of fracture and pore.

$$\begin{aligned} \alpha &= 1 - \frac{K}{K_f}, \\ \beta &= 1 - \frac{K}{K_m}, \end{aligned} \tag{9}$$

where K is the bulk modulus of coal mass $[K = E/3(1-2\mu)]$ (MPa); K_m is the bulk modulus of matrix $[K_m = E_m/3(1-2\mu)]$ (MPa); K_f is the bulk modulus of fracture $[K_f = E_f/3(1-2\mu)]$ (MPa).

The fracture deformation is the combined effect of gas adsorption and effective stress [18]. Therefore, the fracture deformation can be expressed as

$$\Delta\varepsilon_f = \Delta\varepsilon_f^S + \Delta\varepsilon_f^E. \tag{10}$$

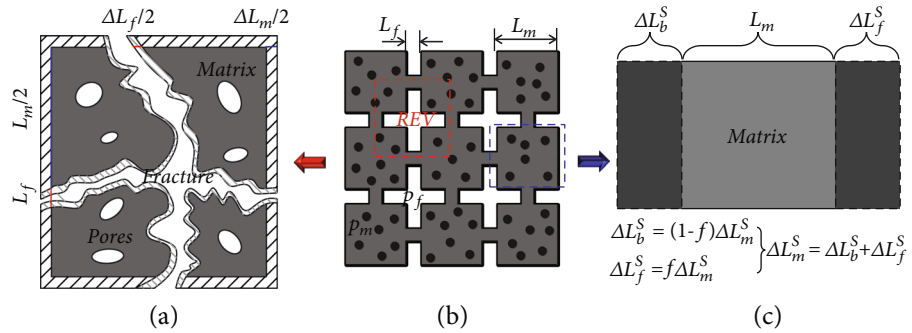

FIGURE 5: Schematic diagram of gas adsorption-induced internal swelling deformation. (a) Representative elementary volume (REV). (b) Coal structure model. (c) Internal swelling deformation caused by gas adsorption.

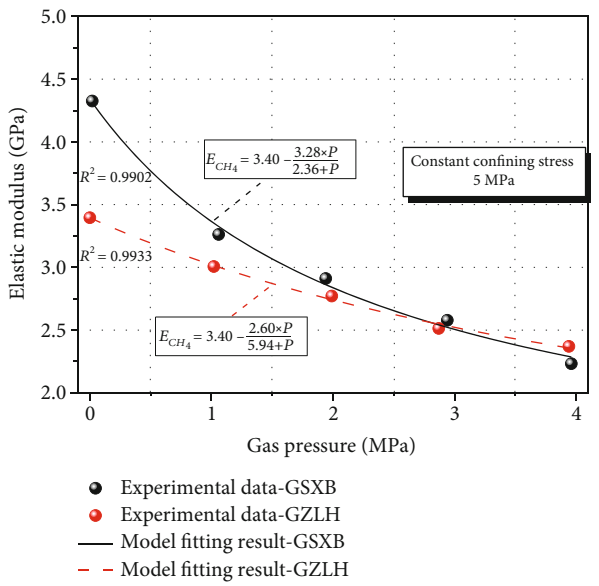

FIGURE 6: Matching results of the dynamic elastic modulus model with laboratory test data under constant external stress conditions.

The deformation influenced by effective stress is expressed as

$$\Delta\varepsilon_f^E = -\frac{\Delta\sigma_e}{K_f}. \tag{11}$$

Substitute Equations (5) and (11) into Equation (10); the fracture deformation can be written as

$$\Delta\varepsilon_f = -\frac{L_m}{L_f} f\varepsilon_L \left(\frac{p_m}{p_L + p_m} - \frac{p_{m0}}{p_L + p_{m0}}\right) - \frac{\Delta\sigma_e}{K_f}. \tag{12}$$

3.2.3. Permeability Equation. Fracture porosity of simplified cube model can be defined as [49]

$$\phi_f = \frac{(L_m + L_f)^3 - L_m^3}{(L_m + L_f)^3} \cong \frac{3L_f}{L_m}. \tag{13}$$

Assume that the matrix size remains constant during coal deformation, and the volume strain of the fracture only changes the fracture aperture, we can obtain

$$\frac{\phi_f}{\phi_{f0}} = \frac{L_f + \Delta L_f}{L_f} = 1 + \Delta\varepsilon_f. \tag{14}$$

Substitute Equation (12) into Equation (14), we obtain

$$\frac{\phi_f}{\phi_{f0}} = 1 - \frac{3f\varepsilon_L}{\phi_{f0}} \left(\frac{p_m}{p_L + p_m} - \frac{p_{m0}}{p_L + p_{m0}}\right) - \frac{\sigma - \sigma_0 - \alpha\left(p_f - p_{f0}\right) - \beta(p_m - p_{m0})}{K_f}. \tag{15}$$

The permeability model is obtained based on Cubic law, it reads [50]

$$\frac{k_f}{k_{f0}} = \left[1 - \frac{3f\varepsilon_L}{\phi_{f0}} \left(\frac{p_m}{p_L + p_m} - \frac{p_{m0}}{p_L + p_{m0}}\right) - \frac{\sigma - \sigma_0 - \alpha\left(p_f - p_{f0}\right) - \beta(p_m - p_{m0})}{K_f}\right]^3. \tag{16}$$

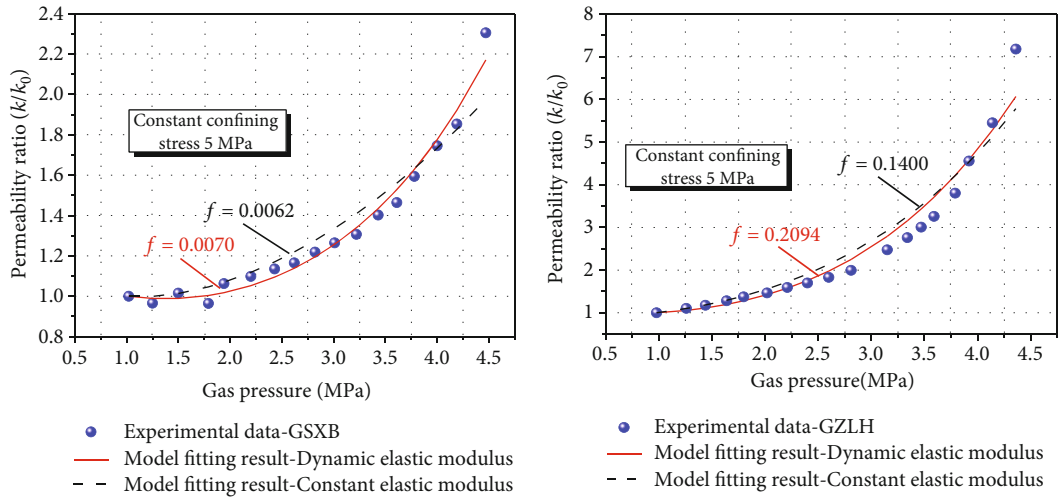

Figure 7: Matching results of the dynamic permeability model with laboratory test data under constant external stress conditions.

Table 3: Parameters used for data matching under constant external stress conditions.

Type	GSXB	GZLH
Langmuir strain constant ε_L	0.01266	0.04
Fracture porosity $\varnothing_{f0}$	0.005	0.003
Langmuir pressure p_L	3.85 MPa	5.94 MPa
Bulk modulus of fracture K_f	9.5 MPa	1.8 MPa
Bulk modulus of matrix K_m	14.3 MPa	20 MPa
Poisson's ratio μ	0.25	0.18

Substitute Equations (2) and (3) into Equation (16), we obtain

$$\frac{k_f}{k_{f0}} = \left[1 - \frac{3f\varepsilon_L}{\phi_{f0}}\left(\frac{p_m}{p_L + p_m} - \frac{p_{m0}}{p_L + p_{m0}}\right) - \frac{\sigma - \sigma_0 - \left(1 - \left((E - \Delta E)/\left(3K_f(1-2\mu)\right)\right)\right)\left(p_f - p_{f0}\right) - \left(1 - \left((E - \Delta E)/\left(3K_m(1-2\mu)\right)\right)\right)(p_m - p_{m0})}{K_f}\right]^3. \tag{17}$$

4. Model Validations

In this section, the validation of the elastic modulus model and permeability model is evaluated against the data sets measured in the laboratory.

4.1. Validation of Elastic Modulus Model. At a constant confining stress of 5.0 MPa, Equation (2) is adopted to fit the data sets measured in the laboratory of two types of coal samples. It can be seen from Figure 6 that the fitting result of GSXB and GZLH is successful, using a least-square regression method with an acceptable coefficient of determination ($R^2 \approx 0.99$). The result indicates that the new elastic modulus model can be used to predict the coal elastic modulus under the conditions of constant confining pressure. From Figure 6, we can see that the elastic modulus of CH_4 saturated coal decreases as the pressure increases. However, the reduction becomes smaller as methane pressure. Based on previous research, it is believed that the reduction in elastic modulus results from the interaction of CH_4 with the coal microstructure. The values of ΔE_{max} and P_E of GZLH are estimated to be 2.60 GPa and 5.94 MPa and GSXB are estimated to be 3.28 GPa and 2.36 MPa, respectively. There is a difference between the two types of coal samples, which

Table 4: Ranges of key parameters.

Reference	Langmuir strain constant (ε_L)	Langmuir pressure constant (P_L) (MPa)	Bulk modulus of fracture (K_f) (MPa)
Seidle and Huitt [50]	0.0136	3.45	1.95-16.13
Harpalani and Chen [22]	0.027	3.45	—
Levine [51]	0.0075-0.0136	4.3-6.3	—
Zahner [52]	0.0051-0.0439	2.1-5.3	—
Mavor and Vaughn [53]	0.0127	4.31	—
Palmer and Mansoori [19]	0.0128	4.31	—
Shi and Durucan [54]	0.01266	2.55, 4.31	3.45-3.76
Shi and Durucan [20]	0.01266	4.31	7.18-10.95
Palmer and Gunter [55]	0.0051-0.0439	2.1-5.31	—
Palmer [56]	0.033	3.45	—
Shi and Durucan [57]	0.01266	4.31	1.72-8.62
Liu and Rutqvist [21]	0.0129	2.55	2.33
Liu et al. [58]	0.01075	4.16	10.87
Liu and Harpalani [59]	—	—	6.67-13.33
Shi et al. [60]	0.01075	4.16	2.06-5.15
Range	*0.0051-0.0439*	*2.1-6.3*	*1.72-16.13*

implies that $\Delta E_{\max}$ will depend on the type, rank, molecular composition, etc. of the coal.

4.2. Validation of Permeability Model. Under the constant external stress condition, the increment of the mean stress equals zero.

$$\sigma - \sigma_0 = 0. \tag{18}$$

Moreover, the permeability evolution is governed by Equation (17). The fitting results are depicted in Figure 7. The parameters used in this paper are listed in Table 3.

From Figure 7, we can see that the dynamic permeability model fits well with the two sets of data. The internal swelling coefficient f of GSXB and GZLH is 0.007898 and 0.2094, respectively. It means 8.98% and 20.94% of the matrix deformation caused by gas adsorption are used to alter the fracture permeability. In addition, it indicates that the internal swelling coefficient corresponding to different coal samples is different.

5. Parameter Sensitivity Analysis

In this section, the parameter sensitivity for the dynamic permeability model under the condition of constant confining pressure was analyzed. GSXB coal sample was selected as the object, and we carried out the parameter sensitivity for its 6 most representative parameters (internal swelling coefficient f, Langmuir strain constant ε_L, initial fracture porosity $\varnothing_{f0}$, Langmuir pressure constant P_L, bulk modulus of fracture K_f, and bulk modulus of matrix K_m).

When analyzing the parameter sensitivity, due to the condition limitation, some parameters cannot be obtained from the field. To make the parameters more representative, we summarized some parameter ranges of the coal samples given by other papers. Then, we used them as the reference during sensitivity analysis. Table 4 depicts the value and the possible ranges of each parameter.

In order to analyze the influence of different parameters on the evolution law of coal permeability, the other parameters were set as constant. The results are shown in Figure 8.

Take the internal swelling coefficient (f) as an example; overall, the internal swelling coefficient (f) has a negative effect on the permeability by influencing the adsorption-induced matrix swelling deformation. As is shown in Figure 8(a), when $f \le 0.005$, coal permeability continues to increase with the pressure. However, when $f \ge 0.005$, coal permeability increases at first and then decreases with the pressure (grey area in the figure). When f is low, the effect of adsorption-induced matrix swelling deformation on the permeability is small. Hence, effective stress plays a leading role in coal permeability. The effective stress increases with pressure, and permeability increases. When f is large enough, the effect of adsorption-induced matrix swelling deformation dominates permeability in the low-pressure range; therefore, the permeability decreases slightly. With the increase of gas pressure, the effect of effective stress is strengthened gradually and the permeability increases. Moreover, the larger pressure, the larger increase of permeability. When the pressure reaches a certain value, effective stress plays the dominant role, and the permeability increases with the pressure.

The Langmuir strain constant ε_L mainly has a negative effect on the permeability by influencing the adsorption-induced matrix swelling deformation. The Langmuir pressure constant P_L has a positive effect on the permeability by influencing the adsorption-induced matrix swelling deformation. The bulk modulus of fracture K_f and the bulk modulus of matrix K_m have a positive effect on the permeability by influencing the effective stress. The initial fracture

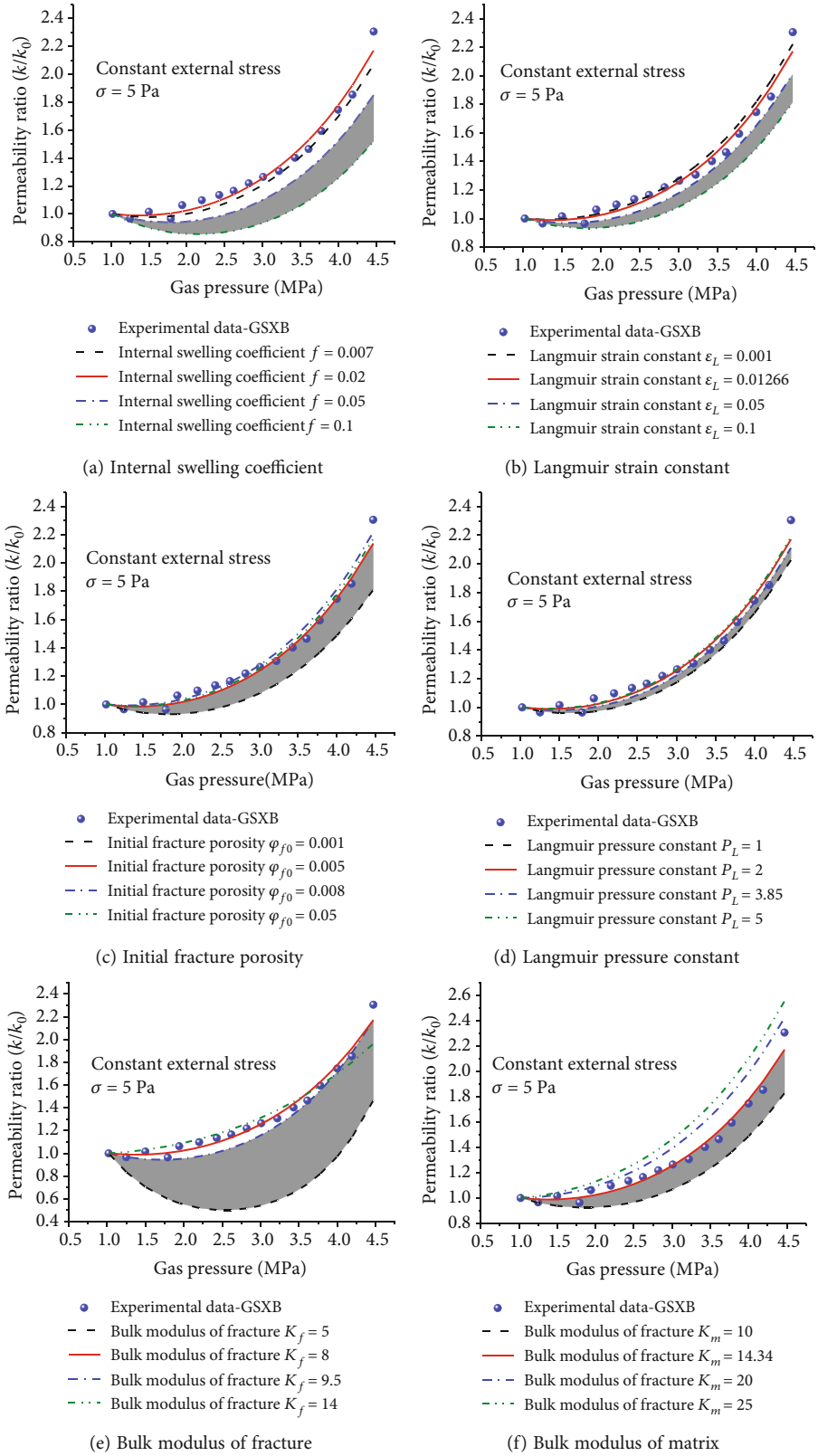

Figure 8: Effect of the different parameters on coal permeability.

porosity $\varnothing_{f0}$ has unknown effects on the permeability by influencing the adsorption-induced matrix swelling deformation, which needed further study.

6. Conclusions

(1) The dynamic elastic modulus model $E_{CH_4} = E - \Delta E$ was obtained through model derivation. Its form indicates that coal elastic modulus shows linear relation with pore pressure. Moreover, with the gas pressure, the elastic modulus gets lower

(2) The dynamic permeability model under the constant confining pressure condition is obtained through model derivation. From the equation structure, it can be known that permeability is affected by both effective stress and adsorption-induced matrix swelling deformation. The third coupling path, namely, the dynamic change of the coal elastic modulus, affects the permeability by changing the effect of effective stress. The elastic modulus under the pore pressure condition is always lower than the initial elastic modulus, which leads to the enhancement of effective stress in the dynamic permeability model. Thus, the inflection point in the pore pressure-permeability figure is not obvious

(3) When validating the parameter sensitivity, different coefficients mainly have three effects, namely, positive effect (Langmuir pressure constant P_L, bulk modulus of fracture K_f, and bulk modulus of matrix K_m), negative effect (internal swelling coefficient f, Langmuir strain constant ε_L), and unknown effect (initial fracture porosity $\varnothing_{f0}$) on the permeability by influencing the adsorption-induced matrix swelling deformation and effective stress

Data Availability

The data used to support the findings of this study are available from the corresponding author upon request.

Conflicts of Interest

The authors declare that they have no conflicts of interest.

Acknowledgments

This work was supported by the Jiangsu Graduate Research and Innovation Project (No. KYCX19_2153 and No. SJKY19_1841).

References

[1] K. Noack, "Control of gas emissions in underground coal mines," *International Journal of Coal Geology*, vol. 35, no. 1–4, pp. 57–82, 1998.

[2] C. Karacan, F. A. Ruiz, M. Cotè, and S. Phipps, "Coal mine methane: a review of capture and utilization practices with benefits to mining safety and to greenhouse gas reduction," *International Journal of Coal Geology*, vol. 86, no. 2-3, pp. 121–156, 2011.

[3] C. Wei, W. Zhu, S. Chen, and P. G. Ranjith, "A coupled thermal-hydrological-mechanical damage model and its numerical simulations of damage evolution in APSE," *Materials*, vol. 9, no. 11, p. 841, 2016.

[4] X. G. H. D. Kong, X. F. Liu, E. Y. Wang et al., "Strain characteristics and energy dissipation laws of gas-bearing coal during impact fracture process," *Energy*, vol. 242, no. 123028, p. 123028, 2022.

[5] T. Liu, B. Lin, X. Fu, and A. Liu, "Mechanical criterion for coal and gas outburst: a perspective from multiphysics coupling," *International Journal of Coal Science & Technology*, vol. 8, no. 6, pp. 1423–1435, 2021.

[6] X. Li, Z. Cao, and Y. Xu, "Characteristics and trends of coal mine safety development," *Energy Sources Part A Recovery Utilization and Environmental Effects*, vol. 12, pp. 1–19, 2020.

[7] M. Pillalamarry, S. Harpalani, and S. Liu, "Gas diffusion behavior of coal and its impact on production from coalbed methane reservoirs," *International Journal of Coal Geology*, vol. 86, no. 4, pp. 342–348, 2011.

[8] G. Ni, Z. Li, and H. Xie, "The mechanism and relief method of the coal seam water blocking effect (WBE) based on the surfactants," *Powder Technology*, vol. 323, pp. 60–68, 2018.

[9] B. Lin, F. Yan, C. Zhu et al., "Cross-borehole hydraulic slotting technique for preventing and controlling coal and gas outbursts during coal roadway excavation," *Journal of Natural Gas Science and Engineering*, vol. 26, pp. 518–525, 2015.

[10] X. Li, S. Chen, S. Wang, M. Zhao, and H. Liu, "Study on in situ stress distribution law of the deep mine: taking Linyi mining area as an example," *Advances in Materials Science and Engineering*, vol. 2021, no. 9, Article ID 5594181, pp. 1–11, 2021.

[11] Q. Zou, B. Lin, C. Zheng et al., "Novel integrated techniques of drilling-slotting-separation-sealing for enhanced coal bed methane recovery in underground coal mines," *Journal of Natural Gas Science and Engineering*, vol. 26, pp. 960–973, 2015.

[12] T. Liu, B. Lin, W. Yang, T. Liu, and C. Zhai, "An integrated technology for gas control and green mining in deep mines based on ultra-thin seam mining," *Environmental Earth Sciences*, vol. 76, no. 6, 2017.

[13] X. Kong, S. Li, E. Wang et al., "Experimental and numerical investigations on dynamic mechanical responses and failure process of gas-bearing coal under impact load," *Soil Dynamics and Earthquake Engineering*, vol. 142, p. 106579, 2021.

[14] Q. Zou, H. Liu, Z. Jiang, and X. Wu, "Gas flow laws in coal subjected to hydraulic slotting and a prediction model for its permeability-enhancing effect," *Energy Sources Part A Recovery Utilization and Environmental Effects*, vol. 7, pp. 1–15, 2021.

[15] Q. Zou, T. Zhang, Z. Cheng, Z. Jiang, and S. Tian, "A method for selection rationality evaluation of the first-mining seam in multi-seam mining," *Geomechanics and Geophysics for Geo-Energy and Geo-Resources*, vol. 8, no. 1, 2022.

[16] X. L. Li, S. J. Chen, S. M. Liu, and Z. H. Li, "AE waveform characteristics of rock mass under uniaxial loading based on Hilbert-Huang transform," *Journal of Central South University*, vol. 28, no. 6, pp. 1843–1856, 2021.

[17] S. Liu, X. Li, D. Wang, and D. Zhang, "Investigations on the mechanism of the microstructural evolution of different coal ranks under liquid nitrogen cold soaking," *Energy Sources Part A Recovery Utilization and Environmental Effects*, vol. 7, pp. 1–17, 2020.

[18] I. Gray, "Reservoir engineering in coal seams: part 1—the physical process of gas storage and movement in coal seams," *SPE Reservoir Engineering*, vol. 2, no. 1, pp. 28–34, 1987.

[19] I. Palmer and J. Mansoori, "How permeability depends on stress and pore pressure in coalbeds: a new model," *SPE Reservoir Evaluation & Engineering*, vol. 1, no. 6, pp. 539–544, 1998.

[20] J. Q. Shi and S. Durucan, "A model for changes in coalbed permeability during primary and enhanced methane recovery," *SPE Reservoir Evaluation & Engineering*, vol. 8, no. 4, pp. 291–299, 2005.

[21] H.-H. Liu and J. Rutqvist, "A new coal-permeability model: internal swelling stress and fracture–matrix interaction," *Transport in Porous Media*, vol. 82, no. 1, pp. 157–171, 2009.

[22] S. Harpalani and G. Chen, "Estimation of changes in fracture porosity of coal with gas emission," *Fuel*, vol. 74, no. 10, pp. 1491–1498, 1995.

[23] C. O. Karacan and G. D. Mitchell, "Behavior and effect of different coal microlithotypes during gas transport for carbon dioxide sequestration into coal seams," *International Journal of Coal Geology*, vol. 53, no. 4, pp. 201–217, 2003.

[24] C. Karacan, "Development and application of reservoir models and artificial neural networks for optimizing ventilation air requirements in development mining of coal seams," *International Journal of Coal Geology*, vol. 72, no. 3-4, pp. 221–239, 2007.

[25] J. W. Larsen, "The effects of dissolved CO_2 on coal structure and properties," *International Journal of Coal Geology*, vol. 57, no. 1, pp. 63–70, 2004.

[26] S. Mazumder, P. V. Hemert, A. Busch, K. Wolf, and P. Tejera-Cuesta, "Flue gas and pure CO_2 sorption properties of coal: a comparative study," *International Journal of Coal Geology*, vol. 67, no. 4, pp. 267–279, 2006.

[27] M. J. Mavor and W. D. Gunter, "Society of Petroleum Engineers SPE annual technical conference and exhibition-Houston," in *SPE Annual Technical Conference and Exhibition-Secondary Porosity and Permeability of Coal vs. Gas Composition and Pressure*, Texas, 2004 September.

[28] B. Mishra and B. Dlamini, "Investigation of swelling and elastic property changes resulting from CO_2 injection into cuboid coal specimens," *Energy & Fuels*, vol. 26, no. 6, pp. 3951–3957, 2012.

[29] M. S. Masoudian, D. W. Airey, and A. El-Zein, "Experimental investigations on the effect of CO_2 on mechanics of coal," *International Journal of Coal Geology*, vol. 128-129, pp. 12–23, 2014.

[30] S. Wang, D. Elsworth, and J. Liu, "Mechanical behavior of methane infiltrated coal: the roles of gas desorption, stress level and loading rate," *Rock Mechanics and Rock Engineering*, vol. 46, no. 5, pp. 945–958, 2013.

[31] L. I. Guofu, L. I. Bo, H. Jiao, and X. Liu, "Three-region integrated CBM stereo-extraction in Jincheng mining area," *China Coalbed Methane*, vol. 11, no. 1, 2014.

[32] J. Li, Q. Huang, G. Wang, and E. Wang, "Influence of active water on gas sorption and pore structure of coal," *Fuel*, vol. 310, p. 122400, 2022.

[33] J. Li, Q. Huang, G. Wang, E. Wang, S. Ju, and C. Qin, "Experimental study of effect of slickwater fracturing on coal pore structure and methane adsorption," *Energy*, vol. 239, p. 122421, 2022.

[34] B. Lin, H. Li, D. Yuan, and Z. Li, "Development and application of an efficient gas extraction model for low-rank high-gas coal beds," *International Journal of Coal Science & Technology*, vol. 2, no. 1, pp. 76–83, 2015.

[35] W. P. Jiang, X. Z. Song, and L. W. Zhong, "Research on the pore properties of different coal body structure coals and the effects on gas outburst based on the lowtemperature nitrogen adsorption method," *Meitan Xuebao/Journal of the China Coal Society*, vol. 36, no. 4, pp. 609–614, 2011.

[36] N. G. Cutmore, B. D. Sowerby, L. J. Lynch, and D. S. Webster, "Determination of moisture in black coal using pulsed nuclear magnetic resonance spectrometry," *Fuel*, vol. 65, no. 1, pp. 34–39, 1986.

[37] L. Song, D. Tang, Z. Pan, X. Hao, and W. Huang, "Characterization of the stress sensitivity of pores for different rank coals by nuclear magnetic resonance," *Fuel*, vol. 111, pp. 746–754, 2013.

[38] G. P. Frosch, J. E. Tillich, R. Haselmeier, M. Holz, and E. Althaus, "Probing the pore space of geothermal reservoir sandstones by nuclear magnetic resonance," *Geothermics*, vol. 29, no. 6, pp. 671–687, 2000.

[39] Y. Yao, D. Liu, and S. Xie, "Quantitative characterization of methane adsorption on coal using a low-field NMR relaxation method," *International Journal of Coal Geology*, vol. 131, pp. 32–40, 2014.

[40] M. S. A. Perera, P. G. Ranjith, and S. K. Choi, "Coal cleat permeability for gas movement under triaxial, non-zero lateral strain condition: a theoretical and experimental study," *Fuel*, vol. 109, pp. 389–399, 2013.

[41] A. Czapliński and S. Hołda, "Changes in mechanical properties of coal due to sorption of carbon dioxide vapour," *Fuel*, vol. 61, no. 12, pp. 1281-1282, 1982.

[42] M. S. Masoudian, D. W. Airey, and A. El-Zein, "A chemo-poro-mechanical model for sequestration of carbon dioxide in coalbeds," *Geotechnique*, vol. 63, no. 3, pp. 235–243, 2013.

[43] D. R. Viete and P. G. Ranjith, "The effect of CO2 on the geomechanical and permeability behaviour of brown coal: implications for coal seam CO_2 sequestration," *International Journal of Coal Geology*, vol. 66, no. 3, pp. 204–216, 2006.

[44] M. Chen and Z. Chen, "Effective stress laws for multi-porosity media," *Applied Mathematics and Mechanics*, vol. 20, no. 11, pp. 1121–1127, 1999.

[45] J. Chen, J. Hopmans, and M. Grismer, "Parameter estimation of two-fluid capillary pressure-saturation and permeability functions," *Advances in Water Resources*, vol. 22, no. 5, pp. 479–493, 1999.

[46] E. P. Robertson and R. L. Christiansen, "A permeability model for coal and other fractured," *Sorptive-Elastic Media. Spe Journal*, vol. 13, no. 3, pp. 314–324, 2006.

[47] T. Liu, B. Lin, and W. Yang, "Impact of matrix-fracture interactions on coal permeability: model development and analysis," *Fuel*, vol. 207, pp. 522–532, 2017.

[48] Q. Liu, Y. Cheng, W. Li, K. Jin, and W. Zhao, "Mathematical model of coupled gas flow and coal deformation process in low-permeability and first mined coal seam," *Yanshilixue Yu Gongcheng Xuebao/Chinese Journal of Rock Mechanics and Engineering*, vol. 34, pp. 2749–2758, 2015.

[49] Y. Wu, J. Liu, D. Elsworth, H. Siriwardane, and X. Miao, "Evolution of coal permeability: contribution of heterogeneous swelling processes," *International Journal of Coal Geology*, vol. 88, no. 2-3, pp. 152–162, 2011.

[50] J. Seidle and L. Huitt, "Experimental measurement of coal matrix shrinkage due to gas desorption and implications for

cleat permeability increases," in *International meeting on petroleum Engineering*, Beijing, China, 1995OnePetro.

[51] J. R. Levine, "Model study of the influence of matrix shrinkage on absolute permeability of coal bed reservoirs," *Geological Society London Special Publications*, vol. 109, no. 1, pp. 197–212, 1996.

[52] B. Zahner, "Application of material balance to determine ultimate recovery of a San Juan Fruitland coal well," in *SPE annual technical conference and exhibition*, San Antonio, Texas, 1997.

[53] M. J. Mavor and J. E. Vaughn, "99/00885 Increasing coal absolute permeability in the San Juan Basin Fruitland formation," *SPE Reservoir Evaluation & Engineering*, vol. 1, no. 3, pp. 201–206, 1998.

[54] J. Q. Shi and S. Durucan, "Drawdown induced changes in permeability of coalbeds: a new interpretation of the reservoir response to primary recovery," *Transport in Porous Media*, vol. 56, no. 1, pp. 1–16, 2004.

[55] I. M. M. Palmer and B. Gunter, "Permeability changes in coal seams during production and injection," in *International coalbed methane symposium*, University of Alabama Tuscaloosa, Alabama, 2007.

[56] I. Palmer, "Permeability changes in coal: analytical modeling," *International Journal of Coal Geology*, vol. 77, no. 1-2, pp. 119–126, 2009.

[57] J. Q. Shi and S. Durucan, "Exponential growth in San Juan Basin Fruitland coalbed permeability with reservoir drawdown: model match and new insights," *SPE Reservoir Evaluation & Engineering*, vol. 13, no. 6, pp. 914–925, 2010.

[58] S. Liu, S. Harpalani, and M. Pillalamarry, "Laboratory measurement and modeling of coal permeability with continued methane production: part 2 - modeling results," *Fuel*, vol. 94, pp. 117–124, 2012.

[59] S. Liu and S. Harpalani, "Permeability prediction of coalbed methane reservoirs during primary depletion," *International Journal of Coal Geology*, vol. 113, pp. 1–10, 2013.

[60] J.-Q. Shi, S. Durucan, and S. Shimada, "How gas adsorption and swelling affects permeability of coal: a new modelling approach for analysing laboratory test data," *International Journal of Coal Geology*, vol. 128-129, pp. 134–142, 2014.